Lee Seongtaek (Orcid ID: 0000-0001-8954-6103)
Meyer Briana Palmeri (Orcid ID: 0000-0001-6287-9274)
Hernandez-Garcia Luis (Orcid ID: 0000-0003-3002-0304)
Schmit Brian D (Orcid ID: 0000-0002-3616-8388)

Comparison and Optimization of pCASL and VSASL for Rat Thoracolumbar Spinal Cord MRI at 9.4T

Seongtaek Lee[1,3], Briana P Meyer[2,3], Luis Hernandez-Garcia, PhD[4], Shekar N Kurpad, MD, PhD[3,5], Brian D Schmit, PhD[1], and Matthew D Budde, PhD[3,5]

[1]Joint Department of Biomedical Engineering, Marquette University & Medical College of Wisconsin, Milwaukee, WI,
[2]Department of Biophysics, [3]Department of Neurosurgery, Medical College of Wisconsin, Milwaukee, WI,
[4]FMRI Laboratory, Department of Biomedical Engineering, University of Michigan, Ann Arbor, MI,
[5]Clement J. Zablocki Veterans Affairs Medical Center, Milwaukee, WI

Corresponding Author:
Seongtaek Lee
Clement A Zablocki VA Medical Center
VA Medical Center-Research 151
5000 West National Ave
Milwaukee, WI 53295
Email: seongtaek.lee@marquette.edu
Phone: (414) 384-2000 x41533

Running Title: Thoracolumbar SCBF with pCASL and VSASL

Word Counts:

Title: 93 characters (with space)
Abstract: 235 words
Text: 4916 words

Number of Figures: 8
Number of Tables: 1
Number of References: 42

This is the author manuscript accepted for publication and has undergone full peer review but has not been through the copyediting, typesetting, pagination and proofreading process, which may lead to differences between this version and the Version of Record. Please cite this article as doi: 10.1002/mrm.29603

Key words: arterial spin labeling; pseudo-continuous arterial spin labeling; velocity-selective arterial spin labeling; spinal cord injury; multimodal MRI; rat model

Abbreviations

ASL: Arterial Spin Labeling
ATT: Arterial Transit Time
FSL: FMRIB Software Library
LE: Labeling Efficiency
MRI: Magnetic Resonance Imaging
pCASL: Pseudo-Continuous Arterial Spin Labeling
PLD: Post Label Delay
SNR: Signal-to-Noise Ratio
SCBF: Spinal Cord Blood Flow
SCI: Spinal Cord Injury
VSASL: Velocity-Selective Arterial Spin Labeling

Author information

Briana P Meyer
Clement A Zablocki VA Medical Center
VA Medical Center-Research 151
5000 West National Ave
Milwaukee, WI 53295
Email: bmeyer@mcw.edu
Phone: (414) 384-2000 x41533

Luis Hernandez-Garcia
1096 BIRB
2360 Bonisteel Blvd.
Ann Arbor, MI 48109-2108
Email: hernan@umich.edu
Phone: (734) 763-9254

Shekar N Kurpad
Froedtert Hospital

9200 West Wisconsin Avenue,
Milwaukee, WI 53226
Email: skurpad@mcw.edu
Phone: (414) 955-7199

Brian D Schmit
Marquette University
Engineering Hall 344
1637 W Wisconsin Ave
Milwaukee, WI 53233
Email: brian.schmit@marquette.edu
Phone: (414) 288-6125

Matthew D Budde
Clement A Zablocki VA Medical Center
Neuroscience Research Labs - Research 151
5000 West National Ave
Milwaukee, WI 53295
Email: mdbudde@mcw.edu
Phone: (414) 384-2000 x46948

Abstract

Purpose: To evaluate pseudo-continuous arterial spin labeling (pCASL) and velocity-selective arterial spin labeling (VSASL) for quantification of spinal cord blood flow (SCBF) in the rat thoracolumbar spinal cord.

Methods: Labeling efficiency (LE) was compared between pCASL and three VSASL variants in simulations and both phantom and *in vivo* experiments at 9.4T. For pCASL, the effects of label plane position and shimming were systematically evaluated. For VSASL, the effects of composite pulses and phase cycling were evaluated to reduce artifacts. Additionally, vessel suppression, respiratory, and cardiac gating were evaluated to reduce motion artifacts. pCASL and VSASL maps of spinal cord blood flow were acquired with the optimized protocols.

Results: LE of the descending aorta was larger in pCASL compared to VSASL variants. In pCASL, LE off-isocenter was improved by local shimming positioned at the label plane and the anatomical level of labeling for the thoracic cord was only viable at the level of the T10 vertebra. Cardiac gating was essential to reduce motion artifacts. Both pCASL and VSASL successfully demonstrated comparable SCBF values in the thoracolumbar cord.

Conclusion: pCASL demonstrated high and consistent LE in the thoracic aorta, and VSASL was also feasible, but with reduced efficiency. A combination of cardiac gating and recording of actual post-label delays was important for accurate SCBF quantification. These results highlight the challenges and solutions to achieve sufficient ASL labeling and contrast at high field in organs prone to motion.

Key words: arterial spin labeling; pseudo-continuous arterial spin labeling; velocity-selective arterial spin labeling; spinal cord injury; multimodal MRI; rat model

Introduction

Imaging and quantification of perfusion in the spinal cord after injury has the potential to characterize impairment and monitor progressive secondary injury. Arterial spin labeling (ASL) permits non-invasive quantification of perfusion by labeling blood water spins as an endogenous tracer. ASL is an established technique for perfusion measurements of the brain and other organs such as kidney, lung, placenta, and liver (1-4). However, its application to the spinal cord is largely limited to animal models, and few studies of ASL exist in spinal cord injury (SCI) (5-7) despite its potential utility to monitor blood flow changes common after SCI. Pseudo-continuous arterial spin labeling (pCASL) is the recommended MRI approach to measure perfusion in the brain due to its high signal-to-noise ratio (SNR) (8). pCASL employs a train of radiofrequency (RF) pulses to invert spins flowing perpendicular to the labeling plane. pCASL was recently optimized for the rat cervical spinal cord to evaluate spinal cord blood flow (SCBF) as a biomarker for acute SCI (6) by labeling the ascending vertebral arteries. The goal of the current work was to refine ASL methods in the rodent *thoracic* spinal cord. Spinal cord imaging, in general, is vulnerable to artifacts due to bulk motion from the heart, lung, and abdomen, which causes artifacts and degrades labeling efficiency and image quality. Imaging of the thoracic cord experiences increased artifacts and degraded labeling efficiency resulting in poor image quality compared to the cervical cord, likely due to the proximity to the heart and lungs. Therefore, specialized strategies to suppress motion might be important for spinal cord ASL in the thoracic segments, which are often the most-examined region in animal SCI models.

The vasculature of the spinal cord is complex. pCASL depends on a discrete labeling plane located on large feeding arteries. In the thoracic cord, multiple segmental arteries branch from the descending aorta and supply the cord making it difficult to identify a labeling plane for the feeding arteries. Velocity-selective ASL (VSASL) has been proposed (9) to overcome the challenges of labeling plane location, and has been applied successfully in other body organs such as the heart (10,11), kidney (12) and placenta (13). VSASL labels arterial blood with flow faster than a cutoff velocity (V_C) regardless of spatial position. Since it labels blood closer to the target organ, it is less sensitive to transit time effects compared to other ASL techniques. Traditional VSASL has been extensively studied, especially in the brain in which tissues are well-perfused with relatively less motion compared to other organs (9,14-16). Nevertheless, VSASL faces its own technical challenges. It is highly sensitivity to eddy currents and B0/ $B1^+$ inhomogeneity (15,17). Advanced velocity-selective preparation techniques have been developed to minimize these effects, including an eight-segment $B1^+$ insensitive rotation (BIR-8) with symmetric RF and gradient layouts (18). Qin et al. demonstrated improved robustness to B0/ $B1^+$ inhomogeneity and gradient imperfections using the Fourier-transform-based velocity-selective saturation (VSS) (19) and inversion (VSI) techniques (20). Despite the technical

advancements in VSASL (21), its application to the spinal cord and in animals at high field has not been studied.

The main goal of this work was to systematically compare and optimize pCASL and VSASL to measure SCBF in the rat thoracolumbar spinal cord at 9.4T. First, we compared labeling efficiencies between ASL variants in a flow phantom and *in vivo* in the descending aorta, the main feeding artery to the thoracolumbar spinal cord. Next, we evaluated pCASL labeling efficiency based on the label plane position relative to the spine anatomy and magnet isocenter with local or global shim corrections. Next, we aimed to minimize motion artifacts using velocity-encoded vessel suppression, retrospective respiratory gating or prospective cardiac gating. For VSASL, VSS and VSI were further optimized using composite refocusing RF pulses and phase-cycling to remove the stripe artifacts before SCBF quantification. The optimized protocol included either pCASL or VSI labeling with cardiac gating and recording of variable delays for accurate SCBF quantification in the thoracolumbar spinal cord of the rat.

Methods

Animals

All animal procedures were approved by the Institutional Animal Care and Use Committees at the Medical College of Wisconsin and the Clement J. Zablocki Veterans Affairs Medical Center. A total of 3 male and 12 female Sprague-Dawley rats (Charles River Laboratories, Wilmington, MA) with an average weight of 400 g were used for the experiments. Group sizes are reported for each set of results.

Magnetic Resonance Imaging

MRI was performed on a Bruker 9.4T Biospec System (Bruker Biospin, GmbH) operating Paravision version 6.0.1. A 9 cm diameter quadrature volume transmit coil and a 4-channel surface receive coil were centered at isocenter at the T10 thoracic vertebrae. Animals were positioned supine in a custom head holder with a bite bar and ear bars with a respiratory pillow and ECG electrodes for respiratory and cardiac gating, respectively. Rats were anesthetized with 3-4% isoflurane and maintained at 2-3% during imaging with a target of 40-50 breaths per minute for stable physiology. Animal body temperature was maintained at 37° ± 1° with heated air.

Arterial Spin Labeling

Four ASL variants were evaluated as described in Figure 1. pCASL labeling used parameters identical to prior optimization in the rodent spinal cord (6): 400 μs Hanning pulse, 1 ms repetition time,

$B1_{ave}$=5 μT, G_{max}=45 mT/m, and G_{ave}=5 mT/m. Three VSASL variants were evaluated, with detailed parameters listed in Table 1. BIR-8 used tanh/tan adiabatic RF pulses previously described for diffusion preparation (22) (Table 1). Fourier transform-based velocity-selective saturation (VSS) and inversion (VSI) methods (20) were also used, and included 9 excitation pulses of 10° or 20°, respectively. A pair of refocusing pulses between each excitation pulse followed a MLEV-16 phase cycling scheme (20) was implemented. All VSASL labeling used a V_c of 4 cm/s and velocity encoding gradients parallel to the spinal cord main axis with gradients set to 0 for the control condition.

Labeling efficiency

Labeling efficiency (LE) was first measured in a flow phantom consisting of 4 mm diameter tubing connected to a peristaltic pump placed outside of the magnet room. Flow velocity was measured as 13.5 cm/s using Fourier-based phase contrast angiography, which approximates the mean velocity in the rodent descending aorta (23). Each ASL preparation module was combined with a flow-compensated gradient-echo readout with a short post-label delay (10 ms): TR/TE=509/2.5 ms, resolution=1x1 mm^2, FOV=96x96 mm^2, slice-thickness=8 mm, NEX=1. For pCASL, the labeling plane was perpendicular to the flow direction and positioned at magnet isocenter with a 200 ms label duration.

LE was also evaluated in the descending aorta *in vivo* (N=3). Phase contrast angiography (TR/TE=117.5/3 ms, velocity max=80 cm/s) was acquired with the volume coil in transmit/receive mode to capture the anatomy of the spinal cord, heart, and lungs to highlight the location of the label plane. For LE evaluation, combined respiratory and cardiac gating was used with a trigger occurring 15 ms after the R-R wave to initiate the ASL preparation module with a short post label delay (PLD=5 ms). The pCASL labeling plane was positioned at the T10 vertebral level perpendicular to the descending aorta.

LE was also simulated to evaluate each ASL variant using Matlab (The Mathworks, Inc., Natick, MA) and employing the blochsim set of tools (24,25) with the exact label and control modules incorporating parameters used for *in vivo* experiments. To simulate the phantom experiments, $T_1 \approx T_2$=3400 ms for pure water was used (26), and it was assumed M_z=1 prior to tagging since the tube with flowing water exited the magnet bore. Simulations to replicate the *in vivo* experiments used literature values for arterial blood T_1 (2380 ms) and T_2 (40.8 ms) at 9.4T (27,28). In pCASL, only a small proportion of the overall blood in the animal experiences inversion at the local tagging plane, and therefore M_z=1 was assumed immediately prior to tagging. However, VSASL uses non-selective tagging pulses and the volume coil contained most of the body of the rat. It was therefore assumed that M_z immediately prior to tagging was dependent on the prior spin history. Simulations for VSASL used

multiple repetitions and updated M_z at each step. Label or control conditions used separate repetitions since the label/control experimental images were collected sequentially, and at least 10 TRs were used to reach a steady state to obtain the final simulated LE value.

pCASL Labeling Optimization

pCASL labeling conditions were optimized in the aorta in 6 animals. First, the effect of off-isocenter position was evaluated by maintaining the label plane at vertebral level T10 and repositioning the animal cradle 0, 1, or 2 cm from isocenter and measuring LE at each position. Under these conditions, a global shim was compared to local shimming. For local shimming, a voxel of 2 cm was centered over the intersection of the label plane and the aorta. An automated map-based shimming estimated the appropriate settings up to 2nd order shim values to minimize heterogeneity over the voxel, and this step was redone each time the animal cradle was moved. Subsequently, the effect of anatomical placement of the labeling plane was evaluated by positioning it at vertebral levels between T8 and T10 while keeping the same cradle position. Based on these experiments, the T10 label plane with local shimming consistently demonstrated the highest LE and was used for subsequent pCASL experiments.

For perfusion imaging, pCASL used a longer label duration (1100 ms) along with a global pre-saturation pulse to reset magnetization 2300 ms before the ASL module. Background suppression used an inversion pulse at 1550 ms before imaging to null cerebrospinal fluid (CSF). The acquisition used an 8-shot rapid acquisition with refocused echoes (RARE) readout using center-out k-space line ordering (TR/TE=4000/7 ms, resolution=0.5x0.5 mm^2, FOV=48x32 mm^2, slice-thickness=4 mm). A spatial saturation band was placed anterior to the spinal cord over the aorta for all subsequent experiments. Residual motion artifacts prompted several different motion reduction strategies. First, vessel suppression used a velocity-encoded BIR-8 ASL module immediately prior to image acquisition with the encoding direction parallel to the aorta. Respiratory gating used a prospective gating strategy to discard and immediately repeat an acquisition in which the image was acquired outside of the quiescent respiratory period based on the external respiratory gating signal. Prospective cardiac gating was evaluated by gating the image acquisition after a fixed delay (80 ms) from the R-R wave in addition to a minimal PLD (Figure 2). Since this led to variable PLDs, an external device (LabJack Model U3-LV*, LabJack Corporation, Lakewood, CO*) was connected to the scanner console through a USB and configured with a custom python routine (https://github.com/mdbudde/PVTriggerCapture) to record the actual delays with approximately 1 ms temporal resolution. pCASL images were first acquired across a range of 8 PLDs and 5 NEX in a scan time of 44 minutes. Subsequently, to be consistent with VSASL

acquisitions, 3 PLDs were acquired synchronized to the cardiac cycle period of 200 ms with 4 NEX in a time of 12 minutes.

VSASL optimization

Velocity-selective labeling was combined with the same centric RARE readout used with pCASL. Previous studies (29,30) and initial experiments demonstrated stripe artifacts in VSS and VSI likely caused by imperfect B0/ $B1^+$ homogeneity, which was particularly noticeable with velocity encoding (rostral-caudal) orthogonal to the imaging plane (sagittal). Hard refocusing pulses were first compared to composite (90_x-180_y-90_{-x}) refocusing pulses in both VSS and VSI sequences (31). Additionally, phase cycling was implemented (32,33) which consisted of changing the phase of all composite refocusing pulses relative to the excitation pulses, noting that the MLEV-16 phase cycling of each individual refocusing pulse was maintained. Phase cycling used 0°, 90°, 180°, and 270° increments across successive image label and control pairs, resulting in an effective NEX of 4 per pair. For control of motion in VSASL, the tagging module was cardiac gated and occurred with a delay of 80 ms from the R-R wave, with image acquisition also gated and occurring 80 ms from the R-R wave. Three PLDs were acquired with approximate PLDs equal to 1, 2 or 3 cardiac periods (200, 400, or 600 ms, respectively), and actual PLDs were recorded.

Data Analysis

Data were analyzed using customized Matlab routines. Maps of labeling efficiency were calculated as the difference between label and control ($\Delta M = |(M_L - M_C)|/2M_0$), where M_L and M_C are the complex value for label and control, respectively, and M_0 is the reference proton-density weighted signal acquired with a long TR (6000 ms). To evaluate LE, manual ROIs were drawn as indicated in each figure.

For quantification of spinal cord blood flow (SCBF), the standard kinetic model was used for pCASL (34)

$$SCBF = \frac{6000 \cdot \lambda \cdot \Delta M \cdot e^{\frac{PLD}{T1_b}}}{2 \cdot \alpha \cdot M_0 \cdot T1_b \cdot \left(1 - e^{-\frac{LD}{T1_b}}\right)} \; [ml/100g/min]$$

and for VSI (21)

$$SCBF = \frac{6000 \cdot \lambda \cdot \Delta M \cdot e^{\frac{PLD}{T1_b}}}{2 \cdot \alpha \cdot M_0 \cdot PLD} \; [ml/100g/min]$$

where λ is the blood-brain partition coefficient (0.9 ml/g), ΔM is the pairwise subtracted perfusion-weighted signal between label and control images, and PLD is the post label delay. For pCASL, labeling efficiency (α) was set to 0.88 based on LE simulations of the full sequence. SCBF maps were computed separately for each PLD. For VSI, α was obtained from simulations of the full sequence that included effects of T_2 during the labeling module and the global presaturation pulse and was estimated at 0.58. The longitudinal relaxation time of arterial blood (T_{1b}=2380 ms) used constant values from the literature for 9.4T (6,27). The temporal signal to noise (tSNR) was computed as the mean ΔM divided by the standard deviation across all repetitions. For voxelwise analysis of SCBF, ROIs were determined on the M_0 images that best delineated the spinal cord using FSL (35).

Results

Labeling Efficiency in pCASL and VSASL

pCASL and three VSASL variants were evaluated for labeling efficiency in a flow phantom at 9.4T. In Figure 3A, pCASL showed strong perfusion contrast in the tubing proximal to the labeling plane with consistently high LE values (0.90), consistent with the simulated value of 0.89. VSASL variants showed more spatially extensive labeling since they use global labeling. Among the VSASL methods, VSI had the highest LE (0.99) near its simulated value of 0.97. VSS (0.58) and BIR-8 (0.47) had efficiency values near their simulated values of 0.49 for both methods (Figure 3B). The somewhat larger value for VSS above its theoretical maximum of 0.5 was due to $B1^+$ inhomogeneity, which was estimated through simulations as a $B1^+$ scaling factor of 1.125 within the ROI, noting the same $B1^+$ scaling factor did not substantially change the simulated LE values for VSI (0.96) and BIR8 (0.49).

LE was evaluated in the descending aorta *in vivo* (N=3) (Figure 3C). All methods had lower LE values *in vivo* compared to the flow phantom, with pCASL (0.64 ± 0.21) outperforming the VSASL variants VSI (0.20 ± 0.04), VSS (0.20 ± 0.08), and BIR-8 (0.21 ± 0.06) (Figure 3D). Simulated LE values for pCASL (0.89), VSI (0.24), VSS (0.20), BIR-8 (0.22) were generally consistent with the measured values, and were based on two effects. First, simulations revealed that T_2 relaxation during the VSI, VSS, and BIR-8 modules caused LE to decrease to 0.68, 0.33, and 0.29, respectively, compared to their theoretical maximal values of 1.0 for VSI and 0.5 for VSS and BIR8. Additionally, with the short TR, further reductions in LE were due to limited time for T1 relaxation between successive repetitions. Collectively, both pCASL and VSI were used for further optimization and SCBF quantification, considering the theoretically higher LE of VSI than either of the other saturation methods, BIR8 and VSS.

Optimization of pCASL Labeling Efficiency

The pCASL labeling plane and its effect on LE was evaluated by changing the position of the label plane from isocenter but maintaining its position at the T10 vertebral level and using either a local shim volume over the label plane or the whole-animal global shim settings (N=3) (Figure 4). The localized shimming achieved larger LE at isocenter (0.79 ± 0.06), 1 cm off isocenter (0.79 ± 0.06), and 2 cm off isocenter (0.66 ± 0.08) compared to the global shimming at isocenter (0.57 ± 0.28), 1 cm off isocenter (0.76 ± 0.24), and 2 cm off isocenter (0.62 ± 0.05) (Figure 4C). Local shimming also had lower overall variability and was used for subsequent experiments. Next, the label plane was moved between T8 and T10 using a local shim. LE was largest with low variability at T10 (0.60 ± 0.10) with substantial reductions at T9 (0.27 ± 0.34) or T8 (0.11 ± 0.04) (Figure 4D). Collectively, the results indicated that the label plane at T10, magnet isocenter and local shimming provided the highest LE and least inter-animal variability.

Motion Artifact Suppression and Post-Label Delay (PLD) Monitoring

The optimized pCASL labeling was combined with centric RARE readout to measure SCBF with multiple strategies evaluated to minimize motion artifacts. An inferior saturation pulse anterior (Figure 5A) to the spinal cord was applied to suppress signal from the body and aorta, but the saturation alone did not reduce the ghosting artifacts (Figure 5B). A vessel suppression BIR-8 module was employed immediately prior to image readout but also did not effectively suppress the ghost artifact (Figure 5B). In conjunction with vessel suppression, prospective respiratory gating was evaluated (Figure 5C), but it did not reduce artifacts. Prospective cardiac gating (without respiratory gating) was evaluated and substantially reduced the qualitative ghost artifact. Cardiac gating improved the temporal SNR to 5.32 suggesting cardiac pulsation was the dominant source of the instability (Figure 5D). Cardiac gating alone was used for subsequent experiments.

Since cardiac gating introduces variable delays, the PLD was measured in real time during the entire scan time. In one representative animal shown in Figure 6A, the full set of measured PLDs are plotted compared to the minimum prescribed PLD. Each circle represents one segment from a total of 80 (5 NEX, 8 PLDs, and label/control conditions). For any segment with a PLD above the cutoff criterion of 200 ms which approximately equates to 1 cardiac period, the entire image (all 8 segments) was omitted from SCBF quantification. In the example shown, 7.5% of images were omitted, and the mean difference in PLDs between label and control states was 7.3 ms. In Figure 6B, the individual ΔM images for each PLD were generally devoid of prominent artifacts. Tagged blood was evident in the segmental feeding arteries at the shortest PLD (90 ms), but gradually diminished at longer PLDs. The perfusion signal in the spinal cord did not appreciably change with different PLDs. Across all animals with this protocol (N=6), the normalized perfusion signal ($\Delta M/M_0$) did not vary substantially as a function

of PLD (Figure 6C), principally due to the long label duration (>1100 ms) relative to the expected transit times in the rodent cord. This result led the next set of experiments to a constrained number of PLDs for SCBF quantification in the thoracolumbar cord. Across 6 animals, 17% of images were omitted in SCBF quantification when pCASL scans were collected with 8 PLDs.

Optimization of VSASL

Both VSS and VSI methods using hard (180_y) refocusing pulses suffered from a prominent stripe artifact evident in the label images with orthogonal velocity encoding and imaging directions (Figure 7A). Employing composite (90_x-180_y-90_{-x}) refocusing pulses partially reduced the artifact in VSS but to a lesser degree in VSI (Figure 7). For VSI, phase cycling of the refocusing pulses across different NEX was applied, and complex averaging across all four phase offsets successfully removed the stripe artifacts (Figure 7B). Signal void artifacts were not sufficiently resolved with either composite pulses or phase cycling and were likely related to B0 or $B1^+$ inhomogeneity.

SCBF quantification with pCASL and VSI

Representative SCBF maps using the optimized pCASL and VSI with three PLDs synchronized to the cardiac cycle are shown in Figure 8A. Both methods revealed perfusion contrast in the spinal cord between T11 to L2 as shown in the *ΔM* images with some differences in qualitative image quality and perfusion contrast across the cord, which was also evident in the tSNR maps. PLDs for both techniques were targeted to (200, 400 and 600 ms) to match the expected cardiac period in the rat, and across all animals with this protocol (N=3), resulting in PLDs of 201 ± 101, 340 ± 32, and 535 ± 18 ms for pCASL and 164 ± 14, 365 ± 29, and 560 ± 42 for VSI (Figure 8B). One animal had excessively long PLDs for pCASL, resulting in 4 of 24 images discarded, but all other pCASL and VSI were otherwise within the 1 cardiac period criteria and no images were discarded. tSNR was consistently greater for pCASL at 0.85 ± 0.26, 1.05 ± 0.33, and 1.25 ± 0.32 for the three respective PLDs and 0.64 ± 0.14, 0.89 ± 0.29, 0.72 ± 0.13 for VSI (Figure 8C). SCBF measurements in the cord showed minor trends as a function of PLD, but they did not appreciably differ between pCASL or VSI. The SCBF values measured with pCASL were 76 ± 17, 115 ± 53, and 92 ± 31 ml/100g/min for each PLD and 77 ± 13, 115 ± 43, and 118 ± 13 ml/100g/min for VSI (Figure 8D).

Discussion

This study evaluated pCASL and VSASL (BIR-8, VSS and VSI) for the rat thoracolumbar spinal cord. All methods achieved LE values consistent with simulated values both in a flow phantom and *in*

vivo. *In vivo* labeling efficiency of the velocity-selective methods were estimated to be low. Notably, these *in vivo* LE values are biased by the steady-state effects of the global labeling and the short TR (509 ms) but are less relevant for perfusion imaging methods with a longer TR (4000 ms). The VSASL labeling modules used in this study had echo times of approximately 30-40 ms, which caused T_2 relaxation and reductions in labeling efficiency. For VSI, T_2 relaxation reduced the labeling efficiency to approximately 0.68 of its maximum theoretical value of 1, and in the SCBF experiments the presaturation pulse further reduced overall labeling efficiency to 0.58. This is consistent with the recommended value of 0.56 for human brain applications of VSI (21). The true labeling efficiency may be also affected by additional B0 and $B1^+$ imperfections or other effects such as non-laminar flow.

A main limitation of pCASL, which was clearly realized in these experiments, is the dependence of the labeling plane location. The label plane can be positioned off-isocenter using appropriate phase corrections (36), although maintaining it at isocenter avoids the need for phase correction (37) or calibration strategies (38) that are typically used to minimize magnetic field inhomogeneities. Compared to a global shim, the results presented here demonstrated an effect in favor of a local shimming, which relaxed the constraints of placing the label plane at magnet isocenter. Although in principle a label plane just inferior to the heart would potentially allow perfusion measurements in more superior regions of the cord, we found that label planes at T8 and T9 produced considerably lower LE than at T10, which is likely due to the proximity of the lung. Even local shimming was not able to overcome the high susceptibility differences at these levels. The constraint to T10 is a limitation that complicates future thoracic spinal cord injury animal models in which T8 or T10 injuries are common.

A known challenge with velocity-selective ASL methods, in particular VSS and VSI, is the high sensitivity to B0 and $B1^+$ imperfections. For example, labelling efficiency in a flow phantom was measured at 0.58 for VSS, higher than its theoretical maximum of 0.5 and was caused by an inhomogeneous $B1^+$. Through simulations, the $B1^+$ scaling factor was estimated to be 1.125 within the ROI that accounted for the higher LE value. Under these same conditions, VSI was only marginally affected by the same $B1^+$ inhomogeneity from 0.99 to 0.96, whereas the efficiency of BIR8 did not change as expected since it relies on adiabatic pulses that are insensitive to $B1^+$. $B1^+$ and B0 mapping may be useful in future studies to properly account for these effects in the analysis. Composite refocusing pulses rather than hard pulses were also effective at partially removing the so-called stripe artifacts with VSS but not with VSI. For VSI, phase cycling across different repetitions was necessary to remove the stripes. The culmination of these studies was a VSASL protocol to measure thoracolumbar SCBF in the sagittal plane with minimized artifacts (Figure 8).

Motion of the spinal cord is a complicating factor for most MRI contrasts, but the long label durations and delay times in ASL are particularly challenging. Solutions for timing pulsed ASL across a

range of respiratory periods have been demonstrated (5), but in initial experiments respiratory gating was not sufficient to reduce motion artifacts. Additionally, neither vessel suppression nor a spatial saturation band reduced motion artifacts. Instead, because cardiac motion was the predominant source of motion, and cardiac gating was required to improve tSNR to levels similar to those acceptable for measuring SCBF as in our prior cervical cord study (6). For pCASL, the end of the long label duration is not easily synchronized to the cardiac cycle. Gating introduces variable delay times, and we employed an external device to measure the actual PLDs in real time for retrospective data screening. Since VSASL labeling module durations are shorter (38 ms), an advantage of VSASL was more strict control of cardiac synchronization which permitted PLDs to be very consistently tied to the cardiac rate. Variable delays for both methods may also be complicated by background suppression. For pCASL, a single pre-labeling inversion pulse timed to null CSF was used, and cardiac delays did not vary considerably from the prescribed PLDs, assuming the cardiac rate was consistent. No background suppression was used for VSI, but additional efforts to further optimize it for high field animal systems would be useful, particularly to minimize effects of CSF contamination or pulsation.

In a direct comparison of pCASL and VSASL in the same animals, SCBF was similar quantitatively, although there were notable qualitative differences in the images. Both methods demonstrated contrast in the segmental arteries that supply the spinal canal. pCASL had a larger tSNR compared to VSASL. Both methods had only minor changes in SCBF across different PLDs from one to three cardiac periods. The T13 level had the highest perfusion weighted contrast ($\Delta M/M_0$), although this may be due, in part, to the limited spatial extent of the surface coil. In the rat, the dominant artery supplying the thoracic cord (37), the artery of Adamkiewicz, is typically located at L2-L3 but may be variable in location across animals. A larger coil may be useful to visualize the full thoracic and lumbar spinal cord. pCASL showed a greater apparent difference between tissues, with gray matter having higher perfusion compared to white matter, as expected, although a quantitative comparison was not performed. The contrast between tissues was less evident in the VSI images, which is possibly related to residual artifacts from CSF pulsation. It should be noted that the blood flow values in the rodent brain or spinal cord are consistently greater with ASL compared to invasive measures including microspheres (39) and hydrogen clearance (40,41). A putative explanation is the strong vasodilatory effects of isoflurane, and other anesthetic agents may be important for greater relevance to the awake, normal conditions (42).

Among the limitations of the study, we did not thoroughly investigate the effects of gating delays within the cardiac cycle. Based on prior diffusion MRI of the spinal cord (22), a delay of 80 ms from the R-R wave had the least motion artifacts and highest reproducibility for the image readout period. Beyond its effects on image artifacts, the pulsatility of the major arteries across the cardiac cycle and its

relationship to the velocity cutoff in VSASL may have important considerations to both maximize perfusion contrast and minimize other physiological artifacts such as CSF pulsation. A V_c of 4 cm/s was used in this study based on its use in vessel suppression (8), but a V_c of 2 cm/s is recommended for VSASL applications (21). Another limitation for VSASL in this study was the lack of a second velocity encoding module, which is recommended to constrain the width of the bolus for more accurate quantification. We used only a single velocity module due to the short PLDs and transit times. The effect of multiple VS modules as well as background suppression tailored for animal studies with relatively short transit times needs further examination.

Conclusion

Through systematic evaluation of pCASL and VSASL in the rat, we demonstrated that both methods are viable for noninvasive SCBF monitoring in the thoracolumbar spinal cord. Importantly, pCASL has high and consistent labeling efficiency in the descending aorta, but the label plane was limited to levels below the lung even with local shimming. Cardiac motion caused artifacts that were reduced through cardiac gating and recording of actual PLDs was important for quantification accuracy and reducing outliers. VSASL had an advantage of having more control of cardiac synchronization, resulting in more consistent PLD measurements due to its short label duration. However, the VSI method required a more complex phase cycling to minimize artifacts and had lower labeling efficiency but similar SCBF values as pCASL. Applications to animal models of traumatic spinal cord injury or other disorders affecting the spinal cord are needed to appreciate the implications of perfusion deficits in these models and the utility of VSASL in neurological injuries. This study may also help in guiding the translation of perfusion MRI to human studies with similar motion-compensating strategies.

Acknowledgements

This project was funded by the National Institute of Neurological Disorders and Stroke of the National Institutes of Health under Award Number R01NS109090. The authors thank Matt Runquist and Qian (Kathleen) Yin for their assistance with MRI.

References

1. Echeverria-Chasco R, Vidorreta M, Aramendia-Vidaurreta V, Cano D, Escalada J, Garcia-Fernandez N, Bastarrika G, Fernandez-Seara MA. Optimization of pseudo-continuous arterial spin labeling for renal perfusion imaging. Magn Reson Med 2021;85(3):1507-1521.
2. Shao X, Liu D, Martin T, Chanlaw T, Devaskar SU, Janzen C, Murphy AM, Margolis D, Sung K, Wang DJJ. Measuring human placental blood flow with multidelay 3D GRASE pseudocontinuous arterial spin labeling at 3T. J Magn Reson Imaging 2018;47(6):1667-1676.
3. Seith F, Pohmann R, Schwartz M, Kustner T, Othman AE, Kolb M, Scheffler K, Nikolaou K, Schick F, Martirosian P. Imaging Pulmonary Blood Flow Using Pseudocontinuous Arterial Spin Labeling (PCASL) With Balanced Steady-State Free-Precession (bSSFP) Readout at 1.5T. J Magn Reson Imaging 2020;52(6):1767-1782.
4. Pan X, Qian T, Fernandez-Seara MA, Smith RX, Li K, Ying K, Sung K, Wang DJ. Quantification of liver perfusion using multidelay pseudocontinuous arterial spin labeling. J Magn Reson Imaging 2016;43(5):1046-1054.
5. Duhamel G, Callot V, Decherchi P, Le Fur Y, Marqueste T, Cozzone PJ, Kober F. Mouse lumbar and cervical spinal cord blood flow measurements by arterial spin labeling: sensitivity optimization and first application. Magn Reson Med 2009;62(2):430-439.
6. Meyer BP, Hirschler L, Lee S, Kurpad SN, Warnking JM, Barbier EL, Budde MD. Optimized cervical spinal cord perfusion MRI after traumatic injury in the rat. J Cereb Blood Flow Metab 2021;41(8):2010-2025.
7. Lee S, Wilkins N, Schmit BD, Kurpad SN, Budde MD. Relationships between spinal cord blood flow measured with flow-sensitive alternating inversion recovery (FAIR) and neurobehavioral outcomes in rat spinal cord injury. Magn Reson Imaging 2021;78:42-51.
8. Alsop DC, Detre JA, Golay X, Gunther M, Hendrikse J, Hernandez-Garcia L, Lu H, MacIntosh BJ, Parkes LM, Smits M, van Osch MJ, Wang DJ, Wong EC, Zaharchuk G. Recommended implementation of arterial spin-labeled perfusion MRI for clinical applications: A consensus of the ISMRM perfusion study group and the European consortium for ASL in dementia. Magn Reson Med 2015;73(1):102-116.
9. Wong EC, Cronin M, Wu WC, Inglis B, Frank LR, Liu TT. Velocity-selective arterial spin labeling. Magn Reson Med 2006;55(6):1334-1341.
10. Landes V, Javed A, Jao T, Qin Q, Nayak K. Improved velocity-selective labeling pulses for myocardial ASL. Magn Reson Med 2020;84(4):1909-1918.
11. Franklin SL, Schmid S, Bos C, van Osch MJP. Influence of the cardiac cycle on velocity selective and acceleration selective arterial spin labeling. Magn Reson Med 2020;83(3):872-882.
12. Bones IK, Franklin SL, Harteveld AA, van Osch MJP, Schmid S, Hendrikse J, Moonen C, van Stralen M, Bos C. Exploring label dynamics of velocity-selective arterial spin labeling in the kidney. Magn Reson Med 2021;86(1):131-142.
13. Zun Z, Limperopoulos C. Placental perfusion imaging using velocity-selective arterial spin labeling. Magn Reson Med 2018;80(3):1036-1047.
14. Qiu D, Straka M, Zun Z, Bammer R, Moseley ME, Zaharchuk G. CBF measurements using multidelay pseudocontinuous and velocity-selective arterial spin labeling in patients with long arterial transit delays: comparison with xenon CT CBF. J Magn Reson Imaging 2012;36(1):110-119.
15. Duhamel G, de Bazelaire C, Alsop DC. Evaluation of systematic quantification errors in velocity-selective arterial spin labeling of the brain. Magn Reson Med 2003;50(1):145-153.
16. Wu WC, Wong EC. Intravascular effect in velocity-selective arterial spin labeling: the choice of inflow time and cutoff velocity. Neuroimage 2006;32(1):122-128.

17. Meakin JA, Jezzard P. An optimized velocity selective arterial spin labeling module with reduced eddy current sensitivity for improved perfusion quantification. Magn Reson Med 2013;69(3):832-838.
18. Guo J, Meakin JA, Jezzard P, Wong EC. An optimized design to reduce eddy current sensitivity in velocity-selective arterial spin labeling using symmetric BIR-8 pulses. Magn Reson Med 2015;73(3):1085-1094.
19. Qin Q, Qu Y, Li W, Liu D, Shin T, Zhao Y, Lin DD, van Zijl PCM, Wen Z. Cerebral blood volume mapping using Fourier-transform-based velocity-selective saturation pulse trains. Magn Reson Med 2019;81(6):3544-3554.
20. Qin Q, van Zijl PC. Velocity-selective-inversion prepared arterial spin labeling. Magn Reson Med 2016;76(4):1136-1148.
21. Qin Q, Alsop DC, Bolar DS, Hernandez-Garcia L, Meakin J, Liu D, Nayak KS, Schmid S, van Osch MJP, Wong EC, Woods JG, Zaharchuk G, Zhao MY, Zun Z, Guo J, Group ISS. Velocity-selective arterial spin labeling perfusion MRI: A review of the state of the art and recommendations for clinical implementation. Magn Reson Med 2022;88(4):1528-1547.
22. Lee SY, Meyer BP, Kurpad SN, Budde MD. Diffusion-prepared fast spin echo for artifact-free spinal cord imaging. Magn Reson Med 2021;86(2):984-994.
23. Hartley CJ, Reddy AK, Madala S, Entman ML, Michael LH, Taffet GE. Doppler velocity measurements from large and small arteries of mice. Am J Physiol Heart Circ Physiol 2011;301(2):H269-278.
24. Hargreaves B. Bloch Equation Simulator. http://www-mrsrl.stanford.edu/~brian/blochsim/.
25. Lauzon M. A Beginner's Guide to Bloch Equation Simulations of Magnetic Resonance Imaging Sequences. arXiv preprint arXiv:200902789 2020.
26. Karjalainen J, Henschel H, Nissi MJ, Nieminen MT, Hanni M. Dipolar Relaxation of Water Protons in the Vicinity of a Collagen-like Peptide. J Phys Chem B 2022;126(13):2538-2551.
27. Dobre MC, Ugurbil K, Marjanska M. Determination of blood longitudinal relaxation time (T1) at high magnetic field strengths. Magn Reson Imaging 2007;25(5):733-735.
28. Lee SP, Silva AC, Ugurbil K, Kim SG. Diffusion-weighted spin-echo fMRI at 9.4 T: microvascular/tissue contribution to BOLD signal changes. Magn Reson Med 1999;42(5):919-928.
29. Shin T, Qin Q, Park JY, Crawford RS, Rajagopalan S. Identification and reduction of image artifacts in non-contrast-enhanced velocity-selective peripheral angiography at 3T. Magn Reson Med 2016;76(2):466-477.
30. Shin T, Qin Q. Characterization and suppression of stripe artifact in velocity-selective magnetization-prepared unenhanced MR angiography. Magn Reson Med 2018;80(5):1997-2005.
31. Liu D, Xu F, Li W, van Zijl PC, Lin DD, Qin Q. Improved velocity-selective-inversion arterial spin labeling for cerebral blood flow mapping with 3D acquisition. Magn Reson Med 2020;84(5):2512-2522.
32. Liu D, Li W, Xu F, Zhu D, Shin T, Qin Q. Ensuring both velocity and spatial responses robust to B0/B1+ field inhomogeneities for velocity-selective arterial spin labeling through dynamic phase-cycling. Magn Reson Med 2021;85(5):2723-2734.
33. Qin Q, Shin T, Schär M, Guo H, Chen H, Qiao Y. Velocity-selective magnetization-prepared non-contrast-enhanced cerebral MR angiography at 3 Tesla: Improved immunity to B0/B1 inhomogeneity. Magn Reson Med 2016;75(3):1232-1241.
34. Buxton RB, Frank LR, Wong EC, Siewert B, Warach S, Edelman RR. A general kinetic model for quantitative perfusion imaging with arterial spin labeling. Magn Reson Med 1998;40(3):383-396.
35. Jenkinson M, Beckmann CF, Behrens TE, Woolrich MW, Smith SM. FSL. Neuroimage 2012;62(2):782-790.

36. Dai W, Garcia D, de Bazelaire C, Alsop DC. Continuous flow-driven inversion for arterial spin labeling using pulsed radio frequency and gradient fields. Magn Reson Med 2008;60(6):1488-1497.
37. Larkin JR, Simard MA, Khrapitchev AA, Meakin JA, Okell TW, Craig M, Ray KJ, Jezzard P, Chappell MA, Sibson NR. Quantitative blood flow measurement in rat brain with multiphase arterial spin labelling magnetic resonance imaging. J Cereb Blood Flow Metab 2019;39(8):1557-1569.
38. Luh WM, Talagala SL, Li TQ, Bandettini PA. Pseudo-continuous arterial spin labeling at 7 T for human brain: estimation and correction for off-resonance effects using a Prescan. Magn Reson Med 2013;69(2):402-410.
39. Hickey R, Albin MS, Bunegin L, Gelineau J. Autoregulation of spinal cord blood flow: is the cord a microcosm of the brain? Stroke 1986;17(6):1183-1189.
40. Rubinstein A, Arbit E. Spinal cord blood flow in the rat under normal physiological conditions. Neurosurgery 1990;27(6):882-886.
41. Guha A, Tator CH, Rochon J. Spinal cord blood flow and systemic blood pressure after experimental spinal cord injury in rats. Stroke 1989;20(3):372-377.
42. Hendrich KS, Kochanek PM, Melick JA, Schiding JK, Statler KD, Williams DS, Marion DW, Ho C. Cerebral perfusion during anesthesia with fentanyl, isoflurane, or pentobarbital in normal rats studied by arterial spin-labeled MRI. Magn Reson Med 2001;46(1):202-206.

Table 1. Parameters for the VSASL labeling modules

	T_{VS} (ms)	T_{exc} (ms)	T_{ref} (ms)	T_G (ms)	T_{ramp} (ms)	G_{max} (mT/m)	T_{gap} (ms)	Δ (ms)	V_C (cm/s)
BIR-8	26.60	1.0	2.0	0.4	0.2	55.18	0.25	-	4
VSS	38.67	0.2	1.0	0.4	0.2	34.62	0.25	2.5	4
VSI	38.94	0.2	1.0	0.4	0.2	34.62	0.25	2.5	4

T_{VS}=duration for the entire VS module; T_{exc}=excitation pulse duration; T_{ref}=refocusing pulse duration; T_G=gradient duration; T_{ramp}=gradient ramp time; G_{max}=maximum gradient strength; T_{gap}=duration between gradient and the following RF pulse; Δ=separation between gradient lobes of the same polarity; V_C=cutoff velocity.

Figure Captions

Figure 1. Pulse sequence timing diagrams. A. pCASL pulse sequence timing diagram with non-selective presaturation (3850 ms) and selective inversion (1550 ms) pulses. pCASL module shows two successive RF pulses and gradients for each condition. B. VSASL pulse sequence timing diagram with presaturation (3850 ms) pulse. Symmetric BIR-8 scheme consists of 90-180-180-180-90 adiabatic RF pulses. VSS and VSI have a 180° hard pulse that is broken into nine 10° or 20° segments. For $B1^+$ inhomogeneity correction and off-resonance refocusing, additional 180° pulses were interspersed in between 10° or 20° segments. Velocity-selective gradients are turned off in the control condition for all VSASL variants.

Figure 2. Timing diagram of the post-label delay (PLD) recording system with cardiac gating. Trigger delay is variable based on the cardiac phase after minimum PLD played. Post RR delay is fixed as prescribed by the user (80 ms). PLD is recorded using a LabJack™ device connected to the console TTL (Transitor-Transitor Logic) port and interfaced with Python. Time is recorded at end of labeling period and immediately prior to image acquisition at less than 1 ms temporal resolution.

Figure 3. Flow phantom and *in vivo* labeling efficiency (LE) comparisons. A. A phantom with flowing water and label and control difference images (*ΔM)* for pCASL and VSASL variants. B. Measured and simulated LE in the phantom. C *In vivo ΔM* images of the thoracic aorta. D. Measured and simulated (N=3) LE in the descending aorta. *ΔM* images are scaled differently to highlight contrast for each method. Dashed red rectangles represent the ROI for LE measurements. Bars indicate mean ± standard deviation.

Figure 4. Labeling efficiency (LE) change by label location relative to the magnet isocenter, shim type and vertebral levels. A. Phase contrast angiography acquired to identify the heart, lungs and descending aorta. B. Representative difference images between label and control (*ΔM*) and LE maps using global and localized shim at variable labeling locations. C. Summarized quantitative LE values using different shim strategies at variable labeling locations (N=3). D. Summarized quantitative LE values at T8-T10 vertebral levels using a localized shim (N=3). Dashed squares and blue lines represent localized shim volumes and isocenter, respectively. Dashed red rectangles represent the ROI where the LE was measured. Bars indicate as mean ± standard deviation.

Figure 5. Difference image between label and control (*ΔM*) and temporal signal-to-noise ratio (tSNR) maps with motion suppression (N=1). A. M_0 map of the rat thoracolumbar spinal cord. White box represents an inferior saturation pulse to suppress signal from the body and aorta. Dashed red

rectangles represent the ROI where the tSNR was measured. B. ΔM obtained with vessel suppression (VS) but without any gating. C. ΔM with a retrospective respiratory gating and VS. D. ΔM with a prospective cardiac gating and VS. Total 19 pairs of control and label scans were used to create ΔM and tSNR maps.

Figure 6. Representative PLD measurement with cardiac gating and SCBF quantification using pCASL. A. Comparison between minimum PLD and actual PLD with cardiac gating. Measured PLDs greater than minimum PLD + animal's cardiac period (200 ms) were defined as outliers (red circles). B. Difference image between label and control (ΔM) with varying measured PLDs. C. Mean perfusion weighted contrast ($\Delta M/M_0$) as a function of PLD at T13 across 8 animals. Dashed red rectangles represent the ROI where the $\Delta M/M_0$ was measured.

Figure 7. Removal of the stripe artifacts in velocity-selective saturation (VSS) and inversion (VSI) sequences (N=1). A. The label images of VSS and VSI suffered stripe artifact with hard refocusing pulses (180_y). Using the composite refocusing pulses (90_x-180_y-90_{-x}), the stripes were removed in the VSS label but still remained in VSI label image. B. Stripe artifact in the VSI label was removed by phase cycling the composite refocusing pulses by 90 degrees using an MLEV scheme. M_0 shows the anatomy of the thoracolumbar cord.

Figure 8. The optimized pCASL and VSI (N=3). A. M_0 shows the anatomy of the thoracolumbar cord. Representative maps of ΔM, tSNR and SCBF maps show clear perfusion contrast at each measured PLD. B. Three different PLDs were measured with cardiac gating, resulting in 1, 2, and 3 R-R intervals. C. tSNR was computed at each PLD. D. SCBF was computed at each PLD. SCBF maps were masked by thresholding the M_0 image. Dashed red rectangles show the whole-cord ROIs (T11-L1) used for tSNR and SCBF calculation. Bars indicate as mean ± standard deviation.

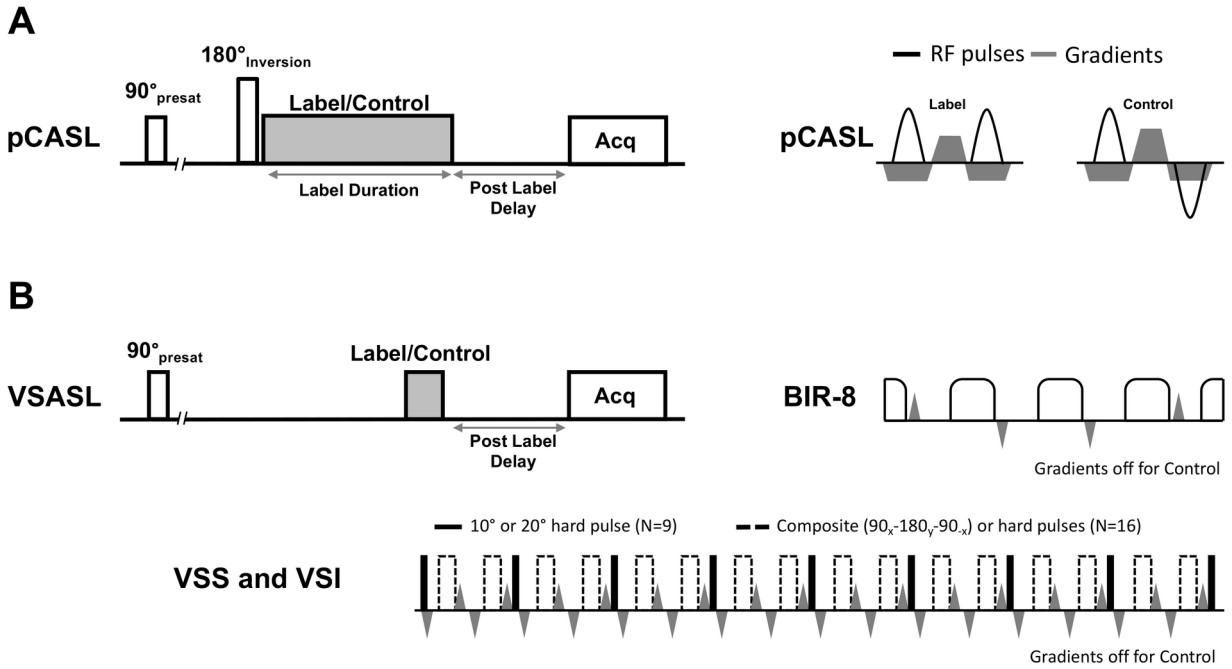

MRM_29603_Figure1.tif

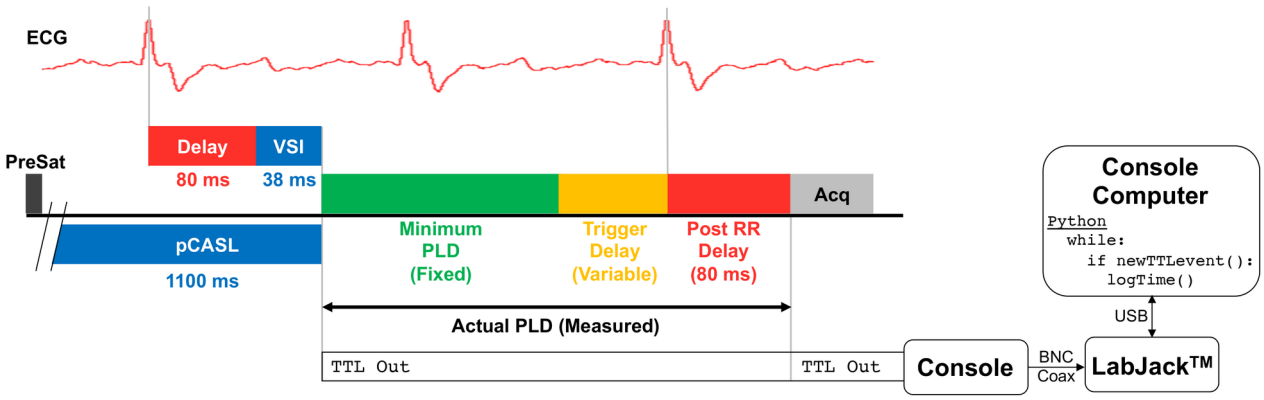

MRM_29603_Figure2.tif

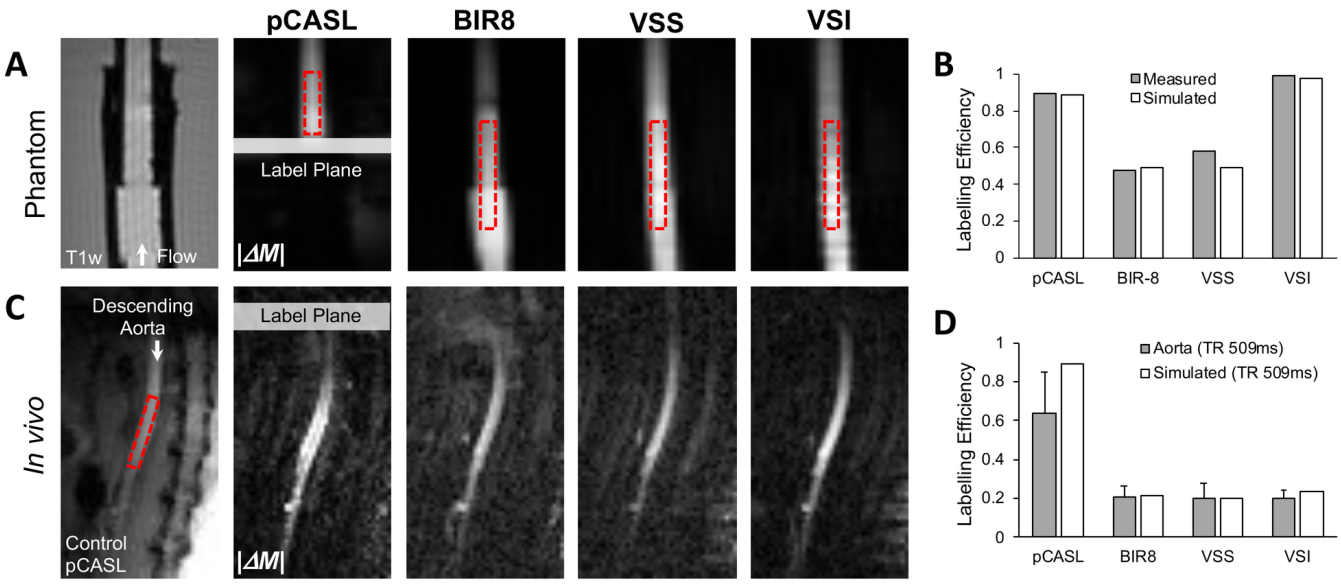

MRM_29603_Figure3.tif

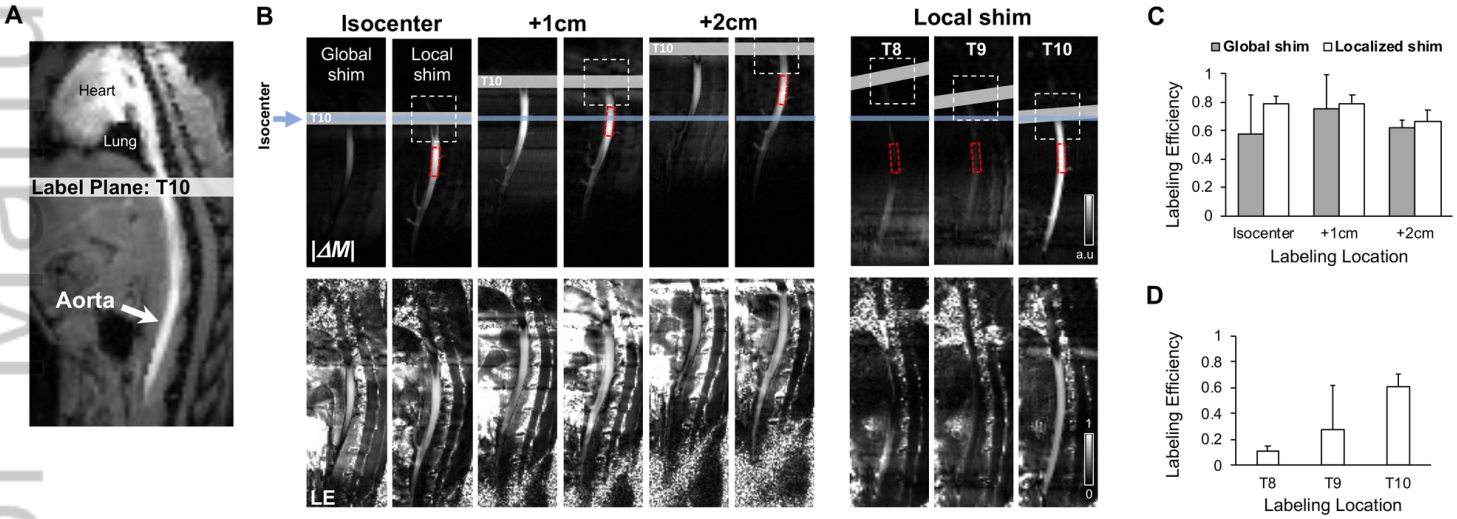

MRM_29603_Figure4.tif

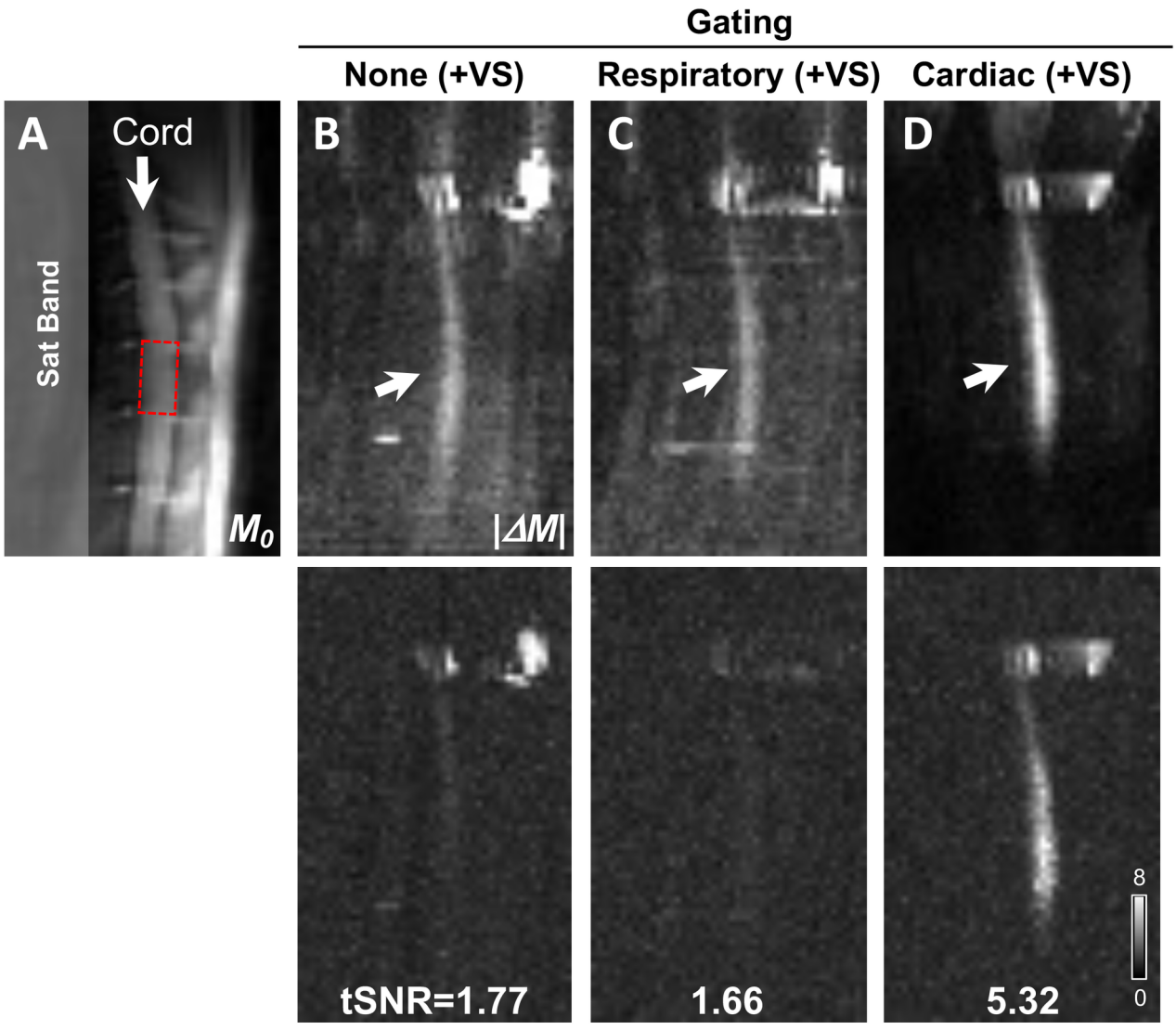

MRM_29603_Figure5.tif

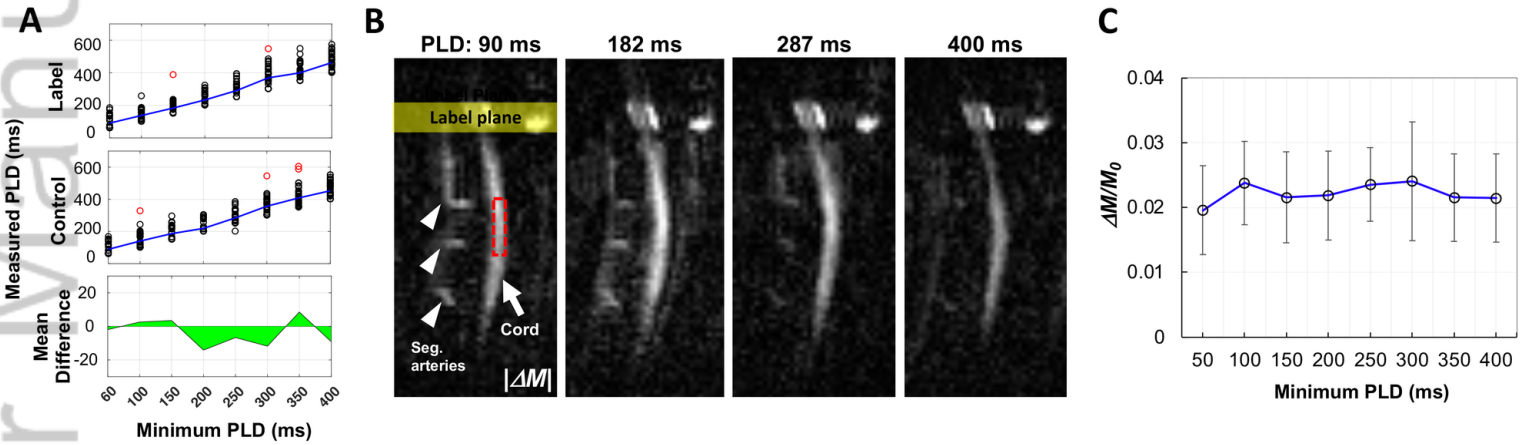

MRM_29603_Figure6.tif

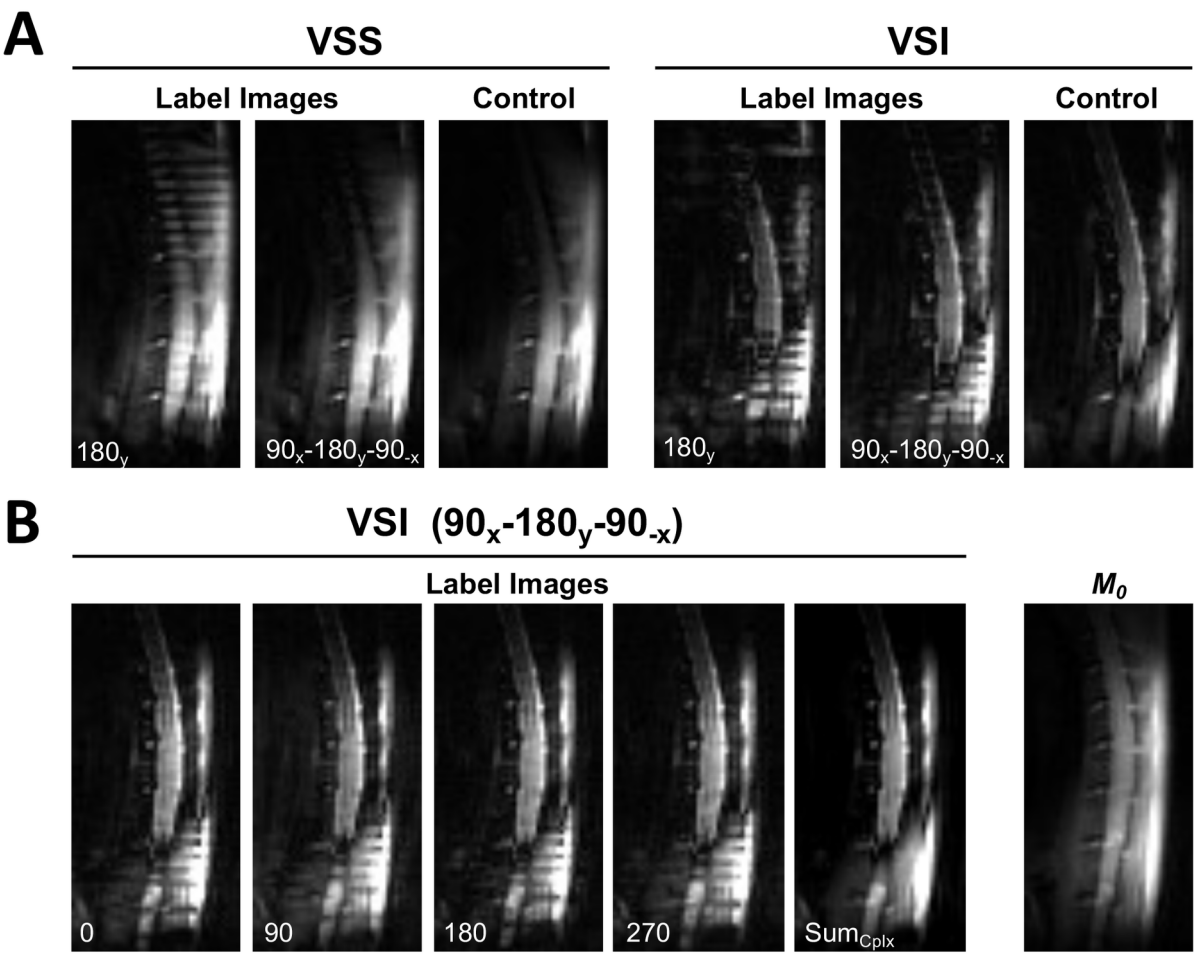

MRM_29603_Figure7.tif

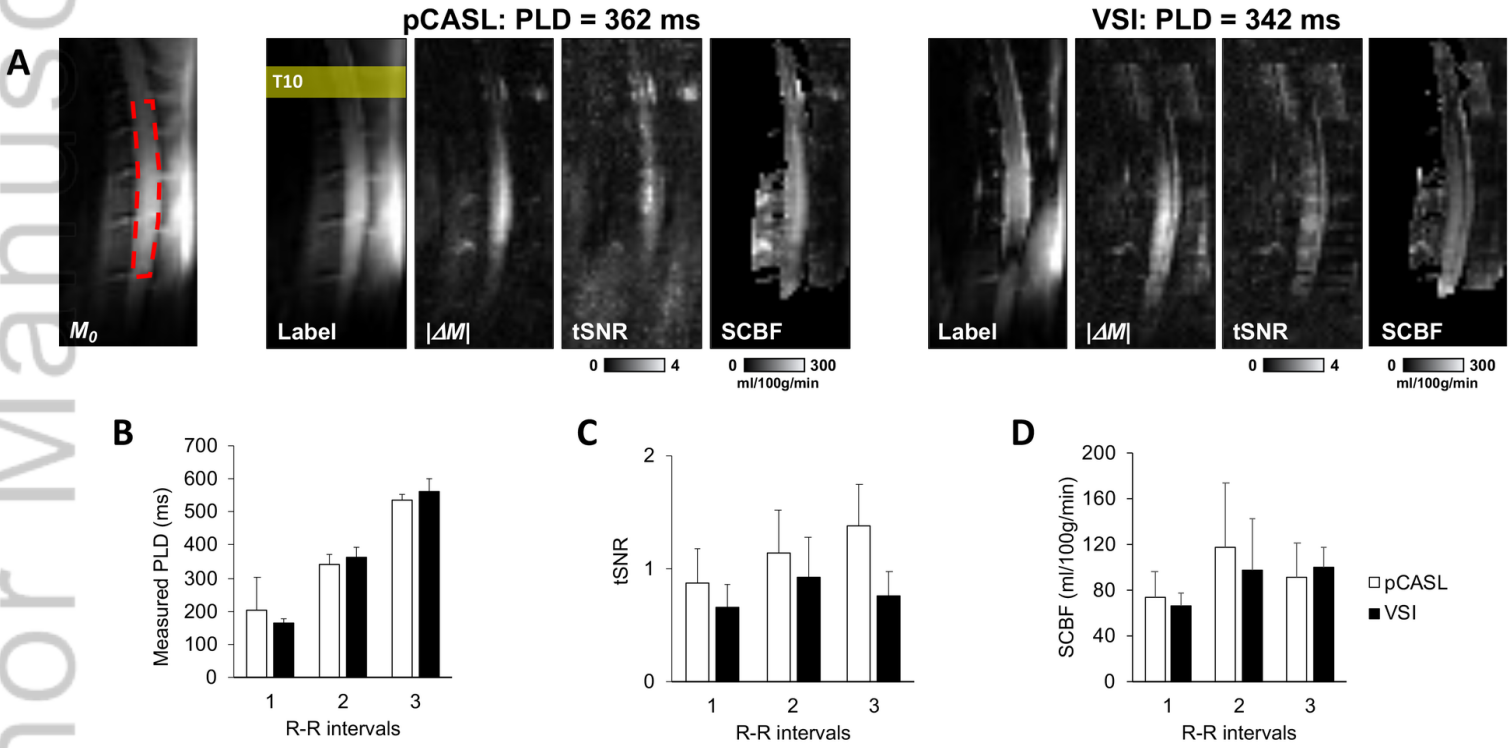

MRM_29603_Figure8.tif